Large area, high responsivity, fast and broadband graphene/n-Si photodetector

Mattia Scagliotti[1,2], Matteo Salvato[1,2,3], Maurizio De Crescenzi[1,2], Neeraj Mishra[4,5], Filippo Fabbri [6], Vaidotas Miseikis[4,5], Camilla Coletti[4,5], Daniele Catone[7], Lorenzo Di Mario[7], Maurizio Boscardin[8] and Paola Castrucci[1,2,]*

[1]Dipartimento di Fisica, Università di Roma 'Tor Vergata', 00133 Roma, Italy

[2]INFN, Università di Roma 'Tor Vergata', 00133 Roma, Italy

[3]CNR-SPIN Salerno, Università degli Studi di Salerno, 84084 Fisciano, Italy

[4] CNI@NEST, Istituto Italiano di Tecnologia, 56127 Pisa, Italy

[5] Graphene Labs, Istituto Italiano di Tecnologia, 16163 Genova, Italy

[6] NEST, Scuola Normale Superiore, Istituto Nanoscienze-CNR, 56127 Pisa, Italy

[7] Istituto di Struttura della Materia-CNR (ISM-CNR), Division of Ultrafast Processes in Materials (FLASHit), 00133 Rome, Italy

[8] Micro-nano Characterization and Fabrication Facility, Fondazione Bruno Kessler (FBK), 38123 Povo-Trento, Italy

*** *Corresponding Author*: Paola Castrucci, email: paola.castrucci@roma2.infn.it**

ABSTRACT

A graphene/silicon heterojunction device has been realized to overcome many different requests necessary to make it a versatile, widely used and competitive detector. The obtained photodetectors which operate at room temperature, are sensitive in the spectral region from the ultraviolet (240 nm) to the infrared (2000 nm) and they can be used in different configurations that allow a high responsivity up to 10^7 A/W, a rise time of a few ns, an external quantum efficiency more than 300%, and a linear response for different light sources. This is allowed by the high quality of the graphene deposited on a large area of 8 mm^2, and by the interdigitated design of the contacts, both preserving the excellent properties of graphene when switching from a nanoscale to the macroscopic dimensions of commonly used devices.

KEYWORDS: Graphene, photodetector, heterojunction, high responsivity, fast response, broadband

1. Introduction

Photodetectors (PDs) are among the most widely used electronic devices in everyday life and in science [1]. They are fundamental, for example, in cameras, smart sensors, surveillance systems, medical devices and weather stations but also in detecting light to directly measure some physical properties or to get information on other types of radiation, e.g. when coupled to a scintillator or a particle attenuator [2]. Each application requires different features of PDs that typically must satisfy strict prerequisites. Among the PD most required characteristics, we can enumerate: its fast response to an external stimulus and to transmit signals; its ability to reveal very weak signals with a great sensitivity and, at the same time, low dark noise; a size large enough to use the PD with

different light sources, both continuous and pulsed, providing a linear response in a large incident power field; its capability to detect signals in a broadband region from ultraviolet (UV) to infrared (IR) radiation; the possibility to work with a low or zero power supply. To satisfy some or all of these requests, in recent years heterostructures based on two-dimensional (2D) and conventional materials have attracted a lot of interest with the main purpose to exploit the unique optoelectronic properties of 2D materials and merge them with those of conventional semiconductors [3]. In this context, graphene/silicon heterojunction (GSH) is emerging [2, 4-9]. The GSH detectors can be easily integrated in the industrial process and in the Si based current technologies, adding features not available in the devices on the market at present [2]. Recently GSH PDs have been able to effectively detect optical signals with wavelengths λ from 380 to 930 nm [10]. The highest responsivity measured in the visible range is around 10^7 A/W with device area equal to 0.025 mm^2 [11]. Other works [12] report on the ability to detect IR radiation with some μs of rise time together with a responsivity approaching 39.5 mA/W. In addition, the fastest devices realized reach response speed of a few ns under λ= 375 nm pulsed laser illumination [13]. Table 1 provides a broad overview of GSH based PDs state of the art. As it is clear, not all the aforementioned characteristics are present in the same device with a large area.

Table 1. Best characteristics of the Gr/Si devices reported in literature

Device	**Spectral Range (nm)**	**Responsivity (A/W)**	**Rise Time (ns)**	**Active Area (mm^2)**	**Ref.**
Gr/ultra-thin Si	200 – 1200	0.46	10^3	$3.6 \cdot 10^{-3}$	[14]
Gr/Si – Gr/SiO_2	360 – 2200	0.27	-	0.85	[4]
Gr/Si	300 - 1100	0.73	$3 \cdot 10^5$	0.1	[6]

Gr/Si	-	88	-	10^{-2}	[7]
Gr/Ele	632 and 1550	10^4	$3 \cdot 10^3$	10^{-2}	[8]
Gr/Si	360 – 1200	0.635	-	0.5	[10]
Gr/Si	200 – 1100	0.435	$1.2 \cdot 10^6$	$5 \cdot 10^{-3}$	[9]
Gr/Si	1500	0.0395	$5 \cdot 10^3$	78	[12]
Gr/Si	200 – 1100	0.2	5	0.25	[13]
Gr/Si	200-1100	10^7	$1.79 \cdot 10^6$	$1 \cdot 10^{-3}$	[11]
Gr/Si	395 – 850	70	-	$6.4 \cdot 10^{-5}$	[15]

In this article, we report on GSH PDs with ultra-fast response of few ns, responsivity as high as 10^7 A/W, optical band in a region from λ=300 nm to λ=2000 nm and a linear response for both continuous and pulsed light sources, all properties which are combined, for the first time, with a large photosensitive area (8 mm^2).

2. Methods

The devices are obtained by depositing graphene on n-doped 100 μm thick crystalline Si substrate (electrical resistivity ρ=0.5 Ω·cm). On one side of the substrate, a 150 nm Cr/Au metallic layer has been evaporated, forming an Ohmic contact with the Si, named Gate (*G*) electrode. On the other side of the Si, two Cr/Pt interdigitated electrodes, have been deposited and kept electrically isolated from the Si substrate by a 300 nm thick SiO_2 template layer. These electrodes, called Source (*S*) and Drain (*D*), are made up of 10 fingers 50 μm wide and 250 μm distant from each other. Graphene was grown via chemical vapor deposition on copper foil with a process similar to that reported in [16] (see Supplementary Material (SM) for further details). It was subsequently transferred on the top of the *S*-*D* electrodes resulting in contact with them and with

the n-Si surface in such a way to give rise to a GSH of area 8 mm^2, which is the photoactive element of the detector. Further information about the transfer procedure can be found in the SM. Upper and lower panels of Figure 1a show the top and side sketches of the device, respectively. Depending on the electrical connections, the device can operate in two different modes: photovoltaic (PV) when the photocurrent is measured between *G* and *S* or *G* and *D* contacts (or potentially between *G* and the short circuited *S*-*D*), and photoconductive (PC) when the photocurrent is measured between *S* and *D* contacts. In this last configuration, the *G* electrode can be used independently for voltage doping [17]. Figure 1b reports an optical image representative of the polycrystalline graphene transferred on pre-patterned substrate. The characterization of the transferred polycrystalline graphene was performed by using scanning Raman spectroscopy. Figure 1c exhibits a representative Raman spectrum of the graphene coated device with the graphene G and 2D Raman peaks at about 1586 cm^{-1} and 2676 cm^{-1}, respectively. The defect-related D-peak at 1352 cm^{-1} is negligible, indicating the high crystalline quality of the material. Raman mapping was performed on an area of 15 x 15 μm^2. The analysis of the histograms of the intensity ratio between the 2D and G peaks, the intensity ratio between the D and G peaks and of the full width at half maximum of the 2D peak indicated the material single-layer nature, low concentration of defects and large size of the single crystalline graphene domains (see SM, for further details and information on Raman set-up, measurements and analysis).

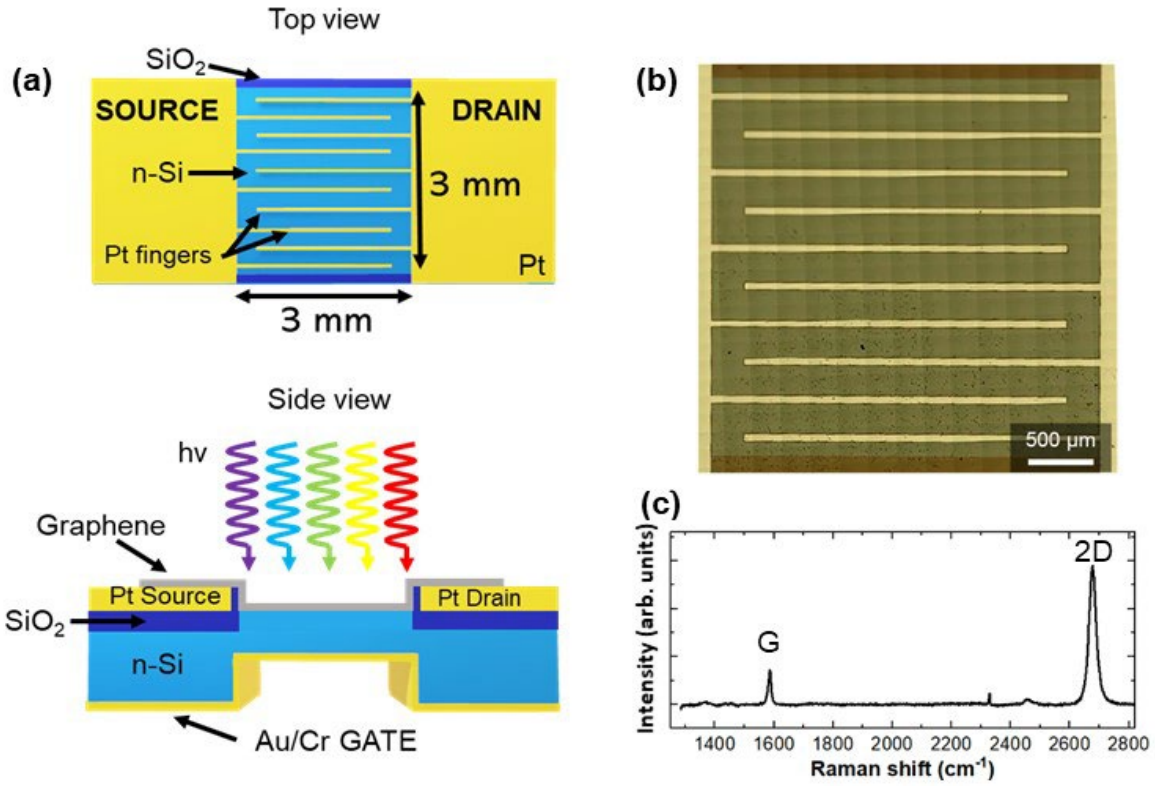

Figure 1. (a) Top (upper panel) and side (lower panel) device schematics. The Gate electrode is realized with a Cr/Au layer evaporated on n-Si. The Source and Drain Pt electrodes are composed by 10 interdigitated combs (large 50 µm and distant 250 µm each other) electrically insulated from the n-Si region through an SiO_2 layer. The graphene film has been deposited on top of Source, Drain and the n-Si area. (b) Optical image of the polycrystalline graphene transferred on pre-patterned substrate. (c) Raman spectrum of the graphene coated device with the graphene G and 2D Raman peaks at about 1586 cm^{-1} and 2676 cm^{-1}, respectively. The defect-related D-peak at 1352 cm^{-1} is negligible, indicating the high crystalline quality of the material.

The devices were characterized by d.c. *I-V* measurements using a Keithley 2602A source/meter lighting it with a solar LOT LSE 140 Xenon lamp. For the responsivity measurements, the PD was illuminated with the solar lamp coupled to a monochromator LOT MSH-300, and the optical power was varied and controlled using attenuators and optical filters. External Quantum Efficiency (EQE)

was acquired using an Ametek 7265 lock-in amplifier after being illuminated by modulated light emitted by the Xenon lamp and passing through the monochromator and a Thorlabs MC 1000A optical chopper system. The time response of the PD devices was investigated using a femtosecond pulsed laser system composed by a chirped pulse amplifier, seeded by a Ti:Sa oscillator which is coupled with an Optical Parameter Amplifier (OPA) [18]. This set-up produces 40 fs wide pulses in a large wavelength range from 240 nm to 20 μm [19, 20]. The current signal is acquired by a 30 GHz Tektronix oscilloscope directly connected with the sample terminals using coaxial cables. Both PV and PC configurations were used for PD characterization. The spot size of any light source here used was always wide enough to illuminate the PD active area completely.

3. Results and discussion

3.1 The photovoltaic configuration

In PV configuration the measured current passes through the graphene/n-Si junction considered as Schottky-type, where graphene acts as a metal and n-Si as semiconductor [21]. Figure 2a shows a typical family of *I-V* characteristics of our PDs acquired in PV mode under different light powers. The forward biased data acquired in dark condition (black line in Figure 2a) are reported in Figure 2b (black dots) in semilogarithmic scale where the low voltage range is fitted (black curve) by the equation [16]:

$$\ln I = \ln I_0 + \frac{e}{\eta k_B T} V \quad (1)$$

valid for Schottky junctions [17]. Here e is the elementary charge, k_B is the Boltzmann constant, T=300K the temperature, η the diode ideality factor and I_0 the leakage current. The fit to the data gives I_0 = 10 nA and η = 1.9. These values qualify the PD device together with Schottky barrier height ϕ_B= 0.80 eV, calculated by the equation $I_0 = AA^*T^2 e^{-\frac{\Phi_B}{k_B T}}$ (where A is the active junction

area and A^*=112 A cm^{-2} K^{-2} is the Richardson constant for Si). All the obtained quantities, ϕ_B included, are comparable to the characteristics of the best GSHs reported in the literature [21], highlighting a high quality of the graphene layer and the effectiveness of the deposition. The higher value of ϕ_B than that expected for an ideal graphene/Si Schottky junction, given the Si substrate doping, the Si electron affinity and the graphene work function, could be due to an ineludible presence of a thin native oxide layer on the Si surface and to inherent not continuous nature of the graphene layer (see SM for details) giving rise to interfacial states as shown theoretically and experimentally in ref. [22] for the graphene/n-GaN junction. In the following, for simplicity, we'll proceed in our discussion by neglecting these interface states and considering an ideal Schottky junction.

When the junction is illuminated, the photons are absorbed within the depletion layer at the interface and electron (e)-hole (h) pairs are formed and separated by the built-in junction potential V_{bi}. A sketch of the band bending at graphene/n-Si interface is given in Figure 2c together with the direction of motion of the photogenerated charges. The electrons travel through the Si and reach the *G* electrode while the holes along the graphene reach the interdigitated *S*-*D* electrodes. As a consequence, the *I*-*V* characteristics shift towards higher values (in module) of the reverse current as reported in Figure 2a and, for the sake of clarity, zoomed in Figure 2d. Here some experimental characteristics are compared to the corresponding theoretical curves (dashed lines in Figure 2d, see SM for calculation details) expected for a generic metallic/semiconducting Schottky junction with the same values of I_0, η and ϕ_B when illuminated by the same light power. Comparing the experimental characteristics with the expected ones, the main difference is in the reverse polarity of the knee voltage V_s at which the current, induced by the photocharge generation, saturates. A rough estimation of its value, obtained by the intercept between the linear extrapolations of the

different slopes of the *I-V* characteristics (see Figure 2a), gives V_s=-0.3V for the 2 mW *I-V* curve, approaching towards the theoretical value in the limit of low power light. This different behavior of the *I-V* characteristics with respect to that expected for a generic metal/semiconductor Schottky PD is already observed by other authors [9] and it is ascribed as peculiar of GSH. At low light intensity, the shape of the *I-V* curve is similar to the one of a conventional photodiode, since all the photogenerated charges can be injected into the graphene finding accessible free states. By increasing the power of the incident light, the number of free electronic states in graphene are no longer sufficient to collect the generated photo charges and therefore there is a strong suppression of the short-circuit current. Such a behavior can therefore be interpreted in terms of a saturation effect due to the electronic structure of graphene [9]. However, a small bias voltage is enough to bring back the *I-V* curve to the ideal shape. Hence by applying an inverse bias voltage, the Fermi level of graphene is shifted, and the number of graphene electronic empty states, arranged to accommodate the photogenerated holes, increases [9]. This is also confermed by the PD power conversion efficiency (PCE) shown in Table 2, which increases by reducing the power illumination. From the analysis of the PCE values, it is worth noting that the PD can operate with no voltage applied in case of lower light power reaching a PCE of 6.37%, while a low (few volts) inverse bias voltage is needed for higher radiation powers. Such a behavior is further reinforced by the following analysis.

Table 2. PCE values extracted from the experimental I-V curves shown in Figure 2d.

P_{opt} (μW)	PCE (%)
20	6.37
632	0.13
1300	0.025
2000	0.003

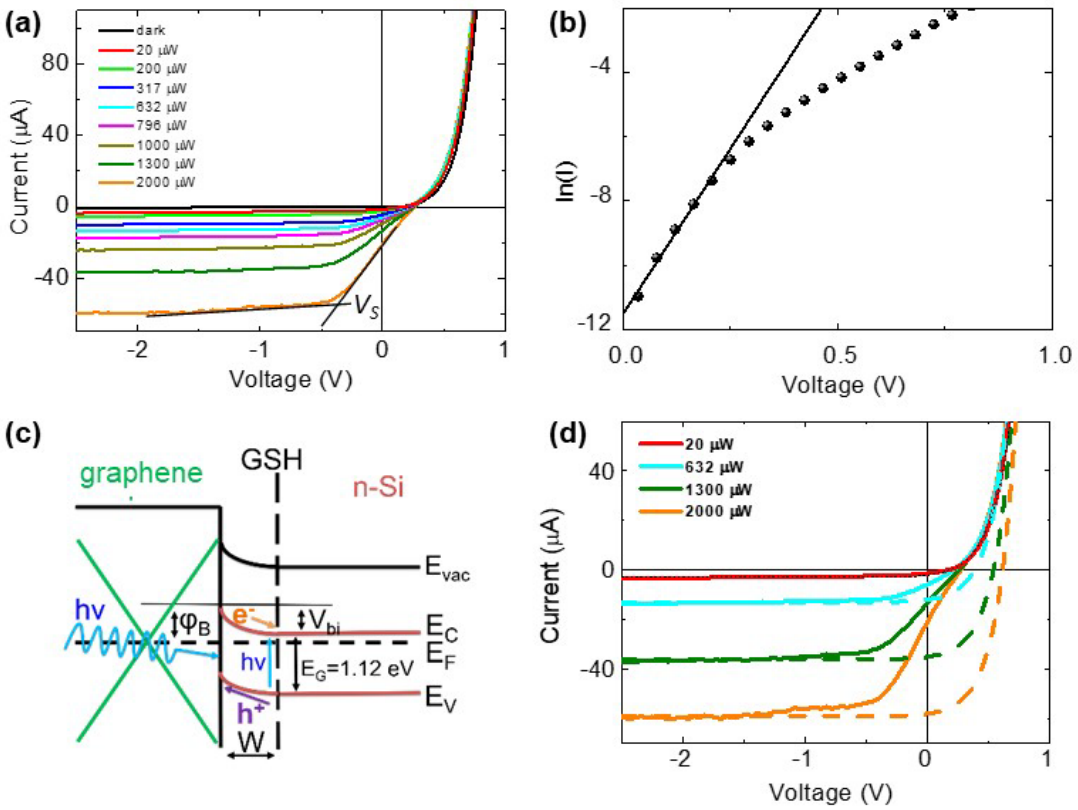

Figure 2. (a) Device I vs V characteristic acquired in Photovoltaic (PV) mode in dark and under several light power conditions. The black lines are linear fit to the data to obtain the knee voltage, V_s, at which the reverse voltage saturates. (b) Device ln(I) vs V characteristic in dark condition (black dots) and linear fit (black curve) at low voltage following equation (1) to extrapolate the ideality factor, η, and leakage current, I_0, values. (c) Band diagram schematics of the graphene/n-Si heterojunction where W represent the depletion layer, V_{bi} the built-in potential and ϕ_B the barrier potential. (d) Enlargement around $V_{DS} = 0$ of some of I-V characteristic (solid curves) of the GSH reported in Figure 2a and the simulated I-V curves (dashed curves) calculated for a generic metallic/semiconducting Schottky junction with the same values of I_0, η and ϕ_B when illuminated by the same light power.

Figure 3a reports the responsivity, $\mathcal{R}$, as a function of the intensity of the incident light with λ = 550 nm measured at different values of bias voltage V_{GS}. $\mathcal{R}$ is defined as $\mathcal{R} = \frac{I_{light} - I_{dark}}{P_{opt}}$ where P_{opt} is the power of the incident light while I_{light} and I_{dark} are the current in conditions of illumination and darkness, respectively. The experimental data confirm the ability of our PDs in detecting monochromatic signals of very low intensity down to few nW. In particular, for the lowest value of P_{opt}, responsivity as high as 0.1 $A \cdot W^{-1}$ is obtained for V_{GS}=0 and a gain of about 4 orders of magnitudes is measured by just applying a low reverse voltage V_{GS}=-2 V. Nonetheless, it is worth noting that the $\mathcal{R}$ values achieved for V_{GS}=0, i.e. without applying any voltage, are of the same order of magnitude of commercial Si-based PDs [23] and are obtained without energy supply and use of any external electronic amplification. In addition, for V_{GS}=0, $\mathcal{R}$ increases of about one order of magnitude up to 1 μW, an incident power value for which it abruptly decreases. While, when a low reverse voltage is applied, the responsivity exhibits a satisfying linear decreasing behavior as a function of the incident light power, P_{opt}, for four orders of magnitude. Indeed, the responsivity curves are well approximated by a power law $y \sim x^{\alpha}$ with the exponent α between 0.8 and 1, thus indicating a satisfying linearity of our PD. The different sign of the rate of $\mathcal{R}$ vs. P_{opt} if a reverse voltage is applied or not, is due to the different slope vs. P_{opt} of the $(I_{light} - I_{dark})$ numerator in the responsivity expression, being almost constant in the former case and steep in the latter. For major details, see Figure S3 in SM where an interpretation of such effects is suggested by considering the presence of an ultra-thin native silicon oxide film at the graphene/silicon junction giving rise to an I_{light} resulting from the difference between the interface hole tunneling current through the oxide toward the graphene and the interface hole recombination current depending on the density of electron interface states under illumination and applied voltage

[24]. In particular, by increasing the reverse applied voltage, the density of electron interface states reduces, thus decreasing the recombination current and increasing I_{light} [24].

In Figure 3b, $\mathcal{R}$ is shown as a function of the wavelength in a spectral range extended from visible (VIS) to near IR, for a number of bias applied voltages $V_{GS,}$ when the device is illuminated by using P_{opt}= 1.3 nW. The $\mathcal{R}$ vs. λ dependence is similar to that obtained for Si PDs [16] for every V_{GS} value, indicating that the main contribution to the photocharge generation comes from the n-Si substrate. Notably, by increasing V_{GS}, the responsivity increases too, reaching its highest values $\mathcal{R}$=7·10^3 A·W^{-1} for V_{GS} = -20 V and λ=750 nm. This behavior is a strong indication that graphene plays the triple role of transparent window, junction constituent and photocharge collector: photons pass through the graphene layer and reach almost unperturbed the Si region. Here the e-h pairs are photogenerated and holes drifted towards the junction under the combined action of the junction potential and V_{GS}. As suggested above, the small applied reverse bias, reduces the recombination current producing a higher I_{light}. At the same time, the higher is the V_{GS} value, the higher is the number of photogenerated holes coming from the silicon substrate able to reach the graphene electrode, due to the increased thickness of the depletion layer, and, contemporary, the number of holes drifted from silicon towards the junction. The former mechanism evidences the typical Si PDs spectral response, while the latter, being incident light wavelength independent, is at the origin of the constant increase of $\mathcal{R}$ over all the impinging photon spectral range.

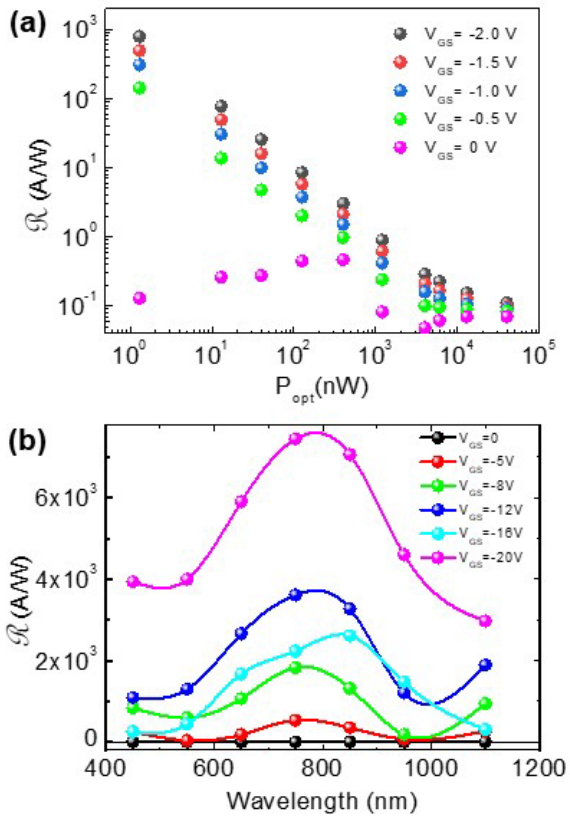

Figure 3. (a) Responsivity, $\mathcal{R}$, in PV mode vs incident 550 nm light power at different bias junction voltage V_{GS}. (b) Responsivity, $\mathcal{R}$, vs incident light wavelength for different applied bias voltage, V_{GS} and incindent light power, P_{opt}= 1.3 nW.

3.2 The photoconductive configuration

In PC mode, the acquisition of the electrical signal takes place between the interdigitated *S* and *D* electrodes. Once the sample is illuminated, this measurement set-up allows to measure the electric current flowing through the graphene consisting of the holes photogenerated near the heterojunction and separated by the junction potential [8, 25]. Furthermore, a voltage can be applied to the gate electrode (V_G) to produce a voltage doping inside graphene. The great enhancement effect of the application of a gate potential on device performance is shown in Figure 4a, where the EQE measurements are reported for different values of V_G. The EQE represents the ratio between the number of photogenerated charges and the number of incident photons on the

device. For V_G=0 the EQE is low, but just using a small V_G> 0, it hugely increases. For V_G=6 V, exceeding 300% EQE values have been obtained in different regions of the spectrum. These good performances are possible thanks to an avalanche effect generated in Si [26]. EQE measurements in Figure 4a are acquired without applying a voltage between the interdigitated electrodes. See Figure S4 in the SM for more details on EQE curve shape. In Figure 4b the value of the responsivity measured at V_G=0 as a function of V_{DS}, for different values of incident light intensity with wavelength λ = 550 nm, are shown. The responsivity can be much increased: with voltage of few volts, values of almost 10^7 $A \cdot W^{-1}$ are reached. These findings can be interpreted in terms of Quantum Charrier Reinvestment (QCR) [11, 15], a mechanism typical in GSH systems where two materials are coupled with different electronic properties. Indeed, by applying a V_G voltage in dark conditions, the I_{DS} vs. V_{DS} feature is measured with a linear trend that represents the measurement of graphene electrical resistance. However, under illumination, photogenerated holes are injected in graphene adding to the free charges present in the dark, and the current value hugely increases. Indeed, incident photons give rise to e-h pairs, which are separated by the graphene/silicon Schottky junction potential and the gate potential. These electric fields drive the photogenerated holes in the graphene and move away photogenerated electrons from the junction. These additional holes have a life time in graphene that depends on their probability to recombine back into silicon: they reach the graphene driven by the junction potential and the gate potential, once in graphene they travel towards the electrodes and then in the external circuit thanks to potential between the interdigitated V_{DS} electrodes. During their life time, thanks to the excellent electronic properties of graphene giving them a very high mobility, the additional holes may circulate several times through the electrodes in the external circuit driven by the applied voltage V_{DS}, thus producing a current quantum gain, *QG*. In our GSH device, the diffusion time of the charges between the *S* and

D electrodes is much lower than their recombination time and this difference is the basis of the current gain and our GSH high responsivity. The quantum gain, *QG*, is defined by the expression $QG = \frac{t_r}{t_t} EQE$ where t_r is the charge recombination time, t_t is the transit time between two adjacent interdigitated electrodes [11]. For V_G=0, EQE=0.03 at λ=550 nm in PC mode. t_t can be calculated considering the charge drift time in graphene $t_t = \frac{d^2}{\mu V_{DS}}$ where d is the distance between the fingers of the PD device (250 μm) and μ is the mobility of the photogenerated charges in the graphene that we assume equal to 10^5 cm^2/V·s [27, 28]. With these values for V_{DS}=6 V, t_t=1·10^{-9} s is obtained. t_r can be estimated by measuring the fall time [29] of the curve shown in Figure 4c, which represents the current response of the PD when it is illuminated by a calibrated pulsed green LED with optical power of 1.2 μW. Assuming for t_r the time required for the signal to decrease from 90% to 10% of its maximum, the value t_r=0.11 ms is obtained. With these values we get a $QG = 3 \cdot 10^3$ which is compatible with the gain value obtained in the $\mathcal{R}$ measurements in Figure 4b for V_{DS}= 6 V and P_{opt}=4 μW. This good match indicates that the value for the mobility in graphene (μ=10^5 cm^2/V·s) used for *QG* estimation, is not far from the true μ in our device, resulting among the best reported in the literature. This finding demonstrates the excellent quality of the deposited graphene layer which, together with the realized design of the interdigitated contacts, allows us to obtain a detector of large active area of 8 mm^2 maintaining the wonderful graphene electronic qualities on large macroscopic scale. Indeed, GSH PD devices often suffer from reduced performance in terms of sensitivity when the active area increases and, as a consequence, the microscopic characteristics of graphene are lost [9].

Responsivity can be further improved by taking advantage of the gate electrode and the effect of voltage doping. In Figure 4d the measure of $\mathcal{R}$ is reported for V_G=0 (black curve) and V_G=18 V (red curve), showing the effect of voltage doping mechanism of, at least, one order of magnitude.

These measurements have been recorded for an incident radiation with optical power of 1 μW and wavelength λ=240 nm.

Detectivity, $\mathcal{D}$, defined as

$$\mathcal{D} = \sqrt{\frac{A}{2eI_{dark}}}\mathcal{R}$$

where A is the device active area and *e* the electron charge, is one of the figure of merit for a PD and indicates the minimum signal that a photodetector can reveal. Interestingly, $\mathcal{D}$ values, corresponding to responsivities reported in Figure 3b, are between 10^{11} and 10^{16} Jones (see for details Figure S6 in the SM) depending on the incident light power and can be further increased by applying a gate voltage V_G. For the case exhibited in Figure 3d, $\mathcal{D}$ values increases of about two orders of magnitude over all the V_{DS} range (see for more details Figure S7 in the SM). Such $\mathcal{D}$ values are competitive with those of commercial PDs [23].

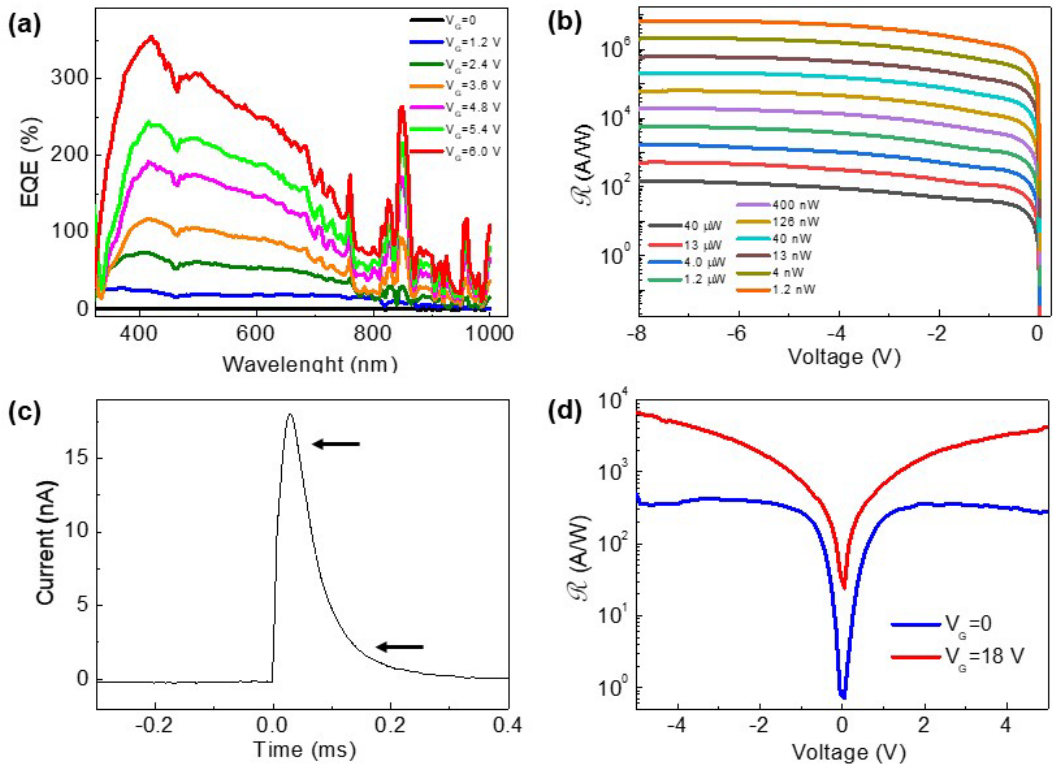

Figure 4. (a) External Quantum Efficiency (EQE) measured between *S* and *D* terminals as a function of the wavelength for different values of V_G with V_{DS}=0. (b) Responsivity, $\mathcal{R}$, in PC mode for V_G=0 under 550 nm illumination at several light powers. (c) PD response to a single peak pulse of a green calibrated LED, the black arrows indicate the 90% and the 10% of the pulse height used as a criterion for the fall time estimation. (d) Responsivity, $\mathcal{R}$, in PC mode vs V_{DS} under 550 nm illumination for V_G=0 (blue line) and V_G=18 V (red line).

3.3 Time-response study

Figure 5a shows the PD response to a 40 fs pulsed laser at different beam energy, tuned at λ=240 nm. Similar behavior is obtained at different wavelengths from the UV (240 nm) up to the IR (2000 nm). The photocurrent, I_{ph}, measured by taking the difference between maximum and minimum in PD response peaks in PV mode with V_{GS}=0 and the laser beam energy E=316 nJ, is

shown in Figure 5b as a function of incident light wavelength, λ. From the reported measurements, it is clear that the device is able to absorb and respond to this broad spectral range and works in a very large incident optical power range, this aspect is a fundamental parameter of the detector. In fact, normally the Si *p-n* junction PDs operate neither in the UV nor in the IR. Indeed, Si absorption coefficient in the UV is very high and therefore UV radiation is mostly absorbed very close to the Si surface [30] where the recombination of the photogenerated charges is very high, thus preventing photo charges to reach the junction (far from the surface at least a few nm). On the other hand, graphene is highly transparent in the visible range and presents an optical absorption peak around 240 nm [13, 31, 32]. These properties produce that UV photons can be absorbed both in graphene and in silicon where the photogenerated *e-h* pairs can safely reach the junction even in the presence of surface recombination, since in the GSH the junction is very close to the surface thanks to the atomic thickness of graphene [14]. As far as the near IR response concerns, conventional Si *p-n* junction PD operation is limited by the band gap energy of silicon around 1060 nm. However, graphene presents interband and intraband transitions enabling optical absorption in the near and medium-far IR, respectively [33, 34]. Therefore, in our PD, graphene not only acts as a transparent window, heterojunction constituent and charge collector, but also as an absorbent photo element. In the region, from about 300 nm to 900 nm, the main contribution of absorption and photocharge collection is provided by Si, while in UV and IR the device absorbs photons thanks to the optical properties of graphene. The photocurrent value, I_{ph}, for some of the measured wavelengths λ in a large energy scale is shown in Figure 5c. For every λ and before the saturation occurs at high light energy, the experimental data are well approximated by a power law $y \sim x^{\alpha}$ with the exponent α between 0.9 and 1.1 confirming the excellent linear response of our PDs. The figure also shows that different energy ranges are necessary to record reliable photocurrent

indicating that the detector results less sensitive to IR with respect to VIS. This happens because the responsible for photodetection in IR is graphene, which has a lower optical absorbance with respect to Si in VIS range. These results demonstrate the great adaptability of our device on a wide energy range, fundamental for using a detector in many different applications.

The time response of the PD is obtained by measuring the rise time τ_r corresponding to the elapsed time between the 10% and 90% of the maximum of each impulse of Figure 5a. This gives values between 10 and 50 ns in PV mode, independent on the laser pulse energy. The PD response can be further improved by operating in PC mode where the signal is collected between the interdigitated electrodes in contact with the graphene [25] and corresponds to the injected photogenerated holes. This is shown in Figure 5d where τ_r is reported as a function of V_G for different wavelengths.

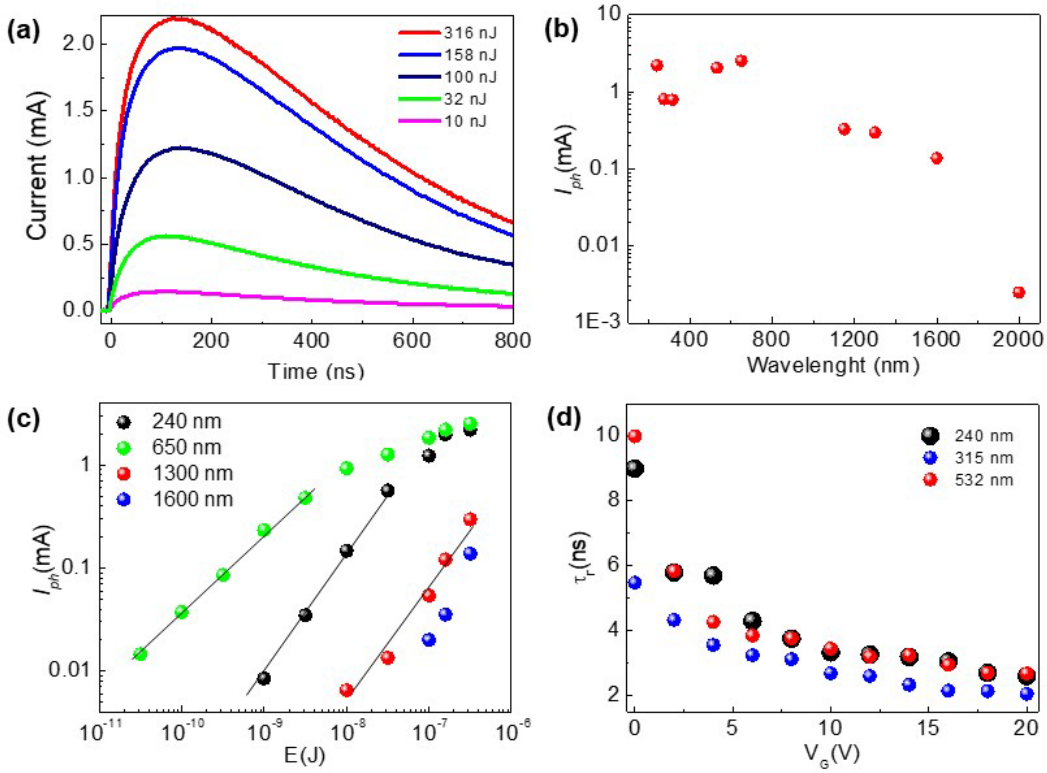

Figure 5. (a) Photocurrent response of the PD to a 40 fs pulsed laser at different beam energy, tuned at photon wavelength, λ=240 nm. (b) Photocurrent difference, I_{ph}, between maximum and

minimum in PD response peaks in PV mode vs. photon wavelength measured with V_{GS}=0 and at incident fs laser light pulse energy E=316 nJ. (c) I_{ph} vs. fs laser light pulse energy measured at different wavelengths in PC mode with V_G=0 and V_{DS}=0; linear curves are fitting obtained by using a power function highlighting the linear behavior as a function of energy at lower laser light pulse energies. (d) Rise time measured in PC mode between 10% and 90% of the rise fronts of the I_{DS} response to the pulsed laser as a function of V_G for different incident wavelengths.

Taking advantage of the voltage doping effect in PC mode, the device becomes faster and 2-5 ns rise time is obtained, making them among the fastest GSH PDs existing in the literature [13, 35]. When V_G is applied, the electric field between the n-Si and the graphene layer, which pushes forward the charges to the electrodes, increases and consequently increases the drift velocity of the injected holes in graphene. These results are possible thanks to the excellent quality of the grown and deposited graphene.

In Table 1, the performances of the best GRH based PDs reported in literature to be compared with the best one of our detector, namely: largest active area of 8 mm^2, wider spectral operation region ranging between 240 and 2000 nm, shortest rise time down to 2 ns and among the highest responsivity in PC mode reaching values up to 10^7 A/W. As it appears clear, our devices are unique in combining high responsivity and fast rise time with large active area.

4. Conclusion

In conclusion, we reported the performance of our photodetector device able to adapt to different sources, with different intensity, frequency and energy. The PD, thanks to the excellent properties of the graphene/n-Si junction, detects light from the UV up to the IR, showing great skill and

adaptability. The deposition of 8 mm square of graphene on Si substrate makes the device a very large active area detector which however maintains the excellent optoelectronic properties of graphene: the PD shows responsivity that reach 10^7 A/W, response times of a few ns, EQE of more than 300%, linear response from 240 nm to 2000 nm and the possibility to use it as self-powered PD or as a three-terminals device using a voltage doping mechanism. Moreover, the device works at room temperature without any post realization treatment to improve its stability.

Acknowledgment

P.C., M.D.C., M.S and M.Sc. would like to acknowledge the European Community for the HORIZON2020 MSC-RISE Project DiSeTCom (GA 823728). N.M., V.M. and C.C. have received funding from the European Union's Horizon 2020 research and innovation program under grant agreement No. 785219 – GrapheneCore2.

References

[1] Konstantatos G 2018 Current status and technological prospect of photodetectors based on two-dimensional materials *Nat Commun* **9** 5266
[2] Long M, Wang P, Fang H and Hu W 2018 Progress, Challenges, and Opportunities for 2D Material Based Photodetectors *Advanced Functional Materials* **29** 1803807
[3] Jariwala D, Marks T J and Hersam M C 2017 Mixed-dimensional van der Waals heterostructures *Nat Mater* **16** 170-81
[4] Riazimehr S, Kataria S, Bornemann R, Haring Bolivar P, Ruiz F J G, Engstrom O, Godoy A and Lemme M C 2017 High Photocurrent in Gated Graphene-Silicon Hybrid Photodiodes *Acs Photonics* **4** 1506-14
[5] Xie C, Wang Y, Zhang Z-X, Wang D and Luo L-B 2018 Graphene/Semiconductor Hybrid Heterostructures for Optoelectronic Device Applications *Nano Today* **19** 41-83
[6] Li X, Zhu M, Du M, Lv Z, Zhang L, Li Y, Yang Y, Yang T, Li X, Wang K, Zhu H and Fang Y 2016 High Detectivity Graphene-Silicon Heterojunction Photodetector *Small* **12** 595-601
[7] Luongo G, Grillo A, Giubileo F, Iemmo L, Lukosius M, Alvarado Chavarin C, Wenger C and Di Bartolomeo A 2019 Graphene Schottky Junction on Pillar Patterned Silicon Substrate *Nanomaterials (Basel)* **9** 659
[8] Chen Z, Cheng Z, Wang J, Wan X, Shu C, Tsang H K, Ho H P and Xu J-B 2015 High Responsivity, Broadband, and Fast Graphene/Silicon Photodetector in Photoconductor Mode *Advanced Optical Materials* **3** 1207-14

[9] An X, Liu F, Jung Y J and Kar S 2013 Tunable graphene-silicon heterojunctions for ultrasensitive photodetection *Nano Lett* **13** 909-16
[10] Riazimehr S, Kataria S, Gonzalez-Medina J M, Wagner S, Shaygan M, Suckow S, Ruiz F G, Engström O, Godoy A and Lemme M C 2018 High Responsivity and Quantum Efficiency of Graphene/Silicon Photodiodes Achieved by Interdigitating Schottky and Gated Regions *Acs Photonics* **6** 107-15
[11] Liu F and Kar S 2014 Quantum Carrier Reinvestment-Induced Ultrahigh and Broadband Photocurrent Responses in Graphene–Silicon Junctions *Acs Nano* **8** 10270-9
[12] Wang C, Dong Y, Lu Z, Chen S, Xu K, Ma Y, Xu G, Zhao X and Yu Y 2019 High responsivity and high-speed 1.55 μm infrared photodetector from self-powered graphene/Si heterojunction *Sensors and Actuators A: Physical* **291** 87-92
[13] Wan X, Xu Y, Guo H, Shehzad K, Ali A, Liu Y, Yang J, Dai D, Lin C-T, Liu L, Cheng H-C, Wang F, Wang X, Lu H, Hu W, Pi X, Dan Y, Luo J, Hasan T, Duan X, Li X, Xu J, Yang D, Ren T and Yu B 2017 A self-powered high-performance graphene/silicon ultraviolet photodetector with ultra-shallow junction: breaking the limit of silicon? *Npj 2d Mater Appl* **1** 4
[14] Ali A, Shehzad K, Guo H, Wang Z, Wang P, Qadir A, Hu W, Ren T, Yu B and Xu Y 2017 High-performance, flexible graphene/ultra-thin silicon ultra-violet image sensor*2-6 Dec. 2017)* p 8.6.1-8.6.4
[15] Chang K E, Yoo T J, Kim C, Kim Y J, Lee S K, Kim S Y, Heo S, Kwon M G and Lee B H 2018 Gate-Controlled Graphene-Silicon Schottky Junction Photodetector *Small* **14** e1801182
[16] Miseikis V, Convertino D, Mishra N, Gemmi M, Mashoff T, Heun S, Haghighian N, Bisio F, Canepa M, Piazza V and Coletti C 2015 Rapid CVD growth of millimetre-sized single crystal graphene using a cold-wall reactor *2d Mater* **2** 014006
[17] Salvato M, Scagliotti M, De Crescenzi M, Crivellari M, Messi R and Castrucci P 2018 Increasing Efficiency in Single-Walled Carbon Nanotube/n-Si Photodetectors by Voltage Doping *IEEE Transactions on Nanotechnology* **17** 837-40
[18] Cerullo G and De Silvestri S 2003 Ultrafast optical parametric amplifiers *Review of Scientific Instruments* **74** 1-18
[19] Tian L, di Mario L, Zannier V, Catone D, Colonna S, O'Keeffe P, Turchini S, Zema N, Rubini S and Martelli F 2016 Ultrafast carrier dynamics, band-gap renormalization, and optical properties of ZnSe nanowires *Phys Rev B* **94**
[20] Toschi F, Catone D, O'Keeffe P, Paladini A, Turchini S, Dagar J and Brown T M 2018 Enhanced Charge Separation Efficiency in DNA Templated Polymer Solar Cells *Advanced Functional Materials* **28** 1707126
[21] Di Bartolomeo A 2016 Graphene Schottky diodes: An experimental review of the rectifying graphene/semiconductor heterojunction *Physics Reports* **606** 1-58
[22] Zhong H J, Xu K, Liu Z H, Xu G Z, Shi L, Fan Y M, Wang J F, Ren G Q and Yang H 2014 Charge transport mechanisms of graphene/semiconductor Schottky barriers: A theoretical and experimental study *J Appl Phys* **115** 013701
[23] Hamamatsu Handbook at. https://www.hamamatsu.com/sp/ssd/doc_en.html.
[24] Song Y, Li X M, Mackin C, Zhang X, Fang W J, Palacios T, Zhu H W and Kong J 2015 Role of Interfacial Oxide in High-Efficiency Graphene-Silicon Schottky Barrier Solar Cells *Nano Lett* **15** 2104-10

[25] Scagliotti M, Salvato M, De Crescenzi M, Kovalchuk N G, Komissarov I V, Prischepa S L, Catone D, Di Mario L, Boscardin M, Crivellari M and Castrucci P 2019 Femtosecond light pulse response of photodetectors based on Graphene/n-Si heterojunctions *Carbon* **152** 643-51
[26] Kobayashi S, Anno Y, Takei K, Arie T and Akita S 2018 Photoresponse of graphene field-effect-transistor with n-type Si depletion layer gate *Sci Rep* **8** 4811
[27] Wang L, Meric I, Huang P Y, Gao Q, Gao Y, Tran H, Taniguchi T, Watanabe K, Campos L M, Muller D A, Guo J, Kim P, Hone J, Shepard K L and Dean C R 2013 One-dimensional electrical contact to a two-dimensional material *Science* **342** 614-7
[28] Pezzini S, Miseikis V, Pace S, Rossella F, Watanabe K, Taniguchi T and Coletti C 2020 High-quality electrical transport using scalable CVD graphene *2d Mater* **7** 041003
[29] Sze S M and Ng K K 2006 *Physics of semiconductor devices*: John wiley & sons)
[30] Green M A 2008 Self-consistent optical parameters of intrinsic silicon at 300K including temperature coefficients *Solar Energy Materials and Solar Cells* **92** 1305-10
[31] Mak K F, Shan J and Heinz T F 2011 Seeing many-body effects in single- and few-layer graphene: observation of two-dimensional saddle-point excitons *Phys Rev Lett* **106** 046401
[32] Kravets V G, Grigorenko A N, Nair R R, Blake P, Anissimova S, Novoselov K S and Geim A K 2010 Spectroscopic ellipsometry of graphene and an exciton-shifted van Hove peak in absorption *Phys Rev B* **81** 155413
[33] Dawlaty J M, Shivaraman S, Strait J, George P, Chandrashekhar M, Rana F, Spencer M G, Veksler D and Chen Y 2008 Measurement of the optical absorption spectra of epitaxial graphene from terahertz to visible *Appl Phys Lett* **93** 131905
[34] Sensale-Rodriguez B, Yan R, Zhu M, Jena D, Liu L and Grace Xing H 2012 Efficient terahertz electro-absorption modulation employing graphene plasmonic structures *Appl Phys Lett* **101** 261115
[35] Selvi H, Hill E W, Parkinson P and Echtermeyer T J 2018 Graphene–silicon-on-insulator (GSOI) Schottky diode photodetectors *Nanoscale* **10** 18926-35